Rapid Intracellular Growth of Gold Nanostructures Assisted by Functionalized Graphene Oxide and Its Application for Surface-Enhanced Raman Spectroscopy

ARTICLE *in* ANALYTICAL CHEMISTRY · OCTOBER 2012

Impact Factor: 5.64 · DOI: 10.1021/ac3023907 · Source: PubMed

5 AUTHORS, INCLUDING:

Zhiming Liu
South China Normal University
30 PUBLICATIONS **438** CITATIONS
SEE PROFILE

Chaofan Hu
Taiyuan University of Technology
17 PUBLICATIONS **457** CITATIONS
SEE PROFILE

Z. Y. Guo
South China Normal University
121 PUBLICATIONS **905** CITATIONS
SEE PROFILE

analytical chemistry

Article

pubs.acs.org/ac

Rapid Intracellular Growth of Gold Nanostructures Assisted by Functionalized Graphene Oxide and Its Application for Surface-Enhanced Raman Spectroscopy

Zhiming Liu,[†] Chaofan Hu,[‡] Shaoxin Li,[§] Wen Zhang,[†] and Zhouyi Guo*[,†]

[†]MOE Key Laboratory of Laser Life Science, College of Biophotonics, South China Normal University, Guangzhou 510631, China

[‡]Department of Chemistry, Jinan University, Guangzhou 510632, China

[§]Guangdong Medical College, Zhanjiang 524023, China

Supporting Information

ABSTRACT: Hybridization of metal nanoparticles with graphene oxide for high performance surface-enhanced Raman scattering (SERS) has attracted overwhelming attention in recent years. Herein, a one-pot green route for intracellular synthesis of gold nanostructures assisted by poly(vinylpyrrolidone) (PVP)-functionalized graphene oxide (GO) was proposed. The hybrids obtained [GO/PVP/intracellularly grown gold nanoparticles (IGAuNs)] randomly scattered throughout the cell. Compared with the IGAuNs, the growth of GO/PVP/IGAuNs was remarkably accelerated, which could be attributed to the coordination of PVP enriched on GO. GO/PVP/IGAuNs could serve as excellent SERS probes for ultrasensitive detection of cellular components of cancer cells located in the cytoplasm, nucleoplasm, and nucleolus. The random intracellular distribution of GO/PVP/IGAuNs facilitated the effective Raman characterization of cellular components, which was confirmed by the uniform distribution of SERS signals in the Raman image. The SERS signals induced by GO/PVP/IGAuNs could be collected as early as 15 h, which allowed rapid detection of tumor cells. In conclusion, this facile and green strategy for fast intracellular growth of GO/PVP/IGAuNs offered great potential for biomedical applications.

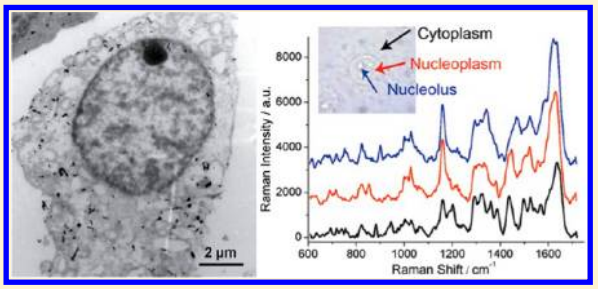

Surface-enhanced Raman scattering (SERS) is a powerful approach to characterize the cellular components,[1] to monitor the intercellular physiological processes,[2] to track the exogenous molecules inside the cell,[3] and to distinguish tumor from the surrounding tissues.[4] Gold and silver nanoparticles (NPs) have been proven to be effective SERS-active substrates due to the excitation of localized surface plasmon resonance around the metallic structures.[5] Traditionally, the metal NPs are delivered into living cells by means of "passive uptake". However, this approach seems to be less effective, taking into account that the plasma membrane functions as a barrier to the exogenous molecules. The endocytosed NPs are often entrapped in lysosomes or endosomes but could not be localized in the nucleus.[6]

Environmentally friendly approaches for NP synthesis without using toxic chemicals are now promising avenues of research in nanoscience. Biosynthetic methods employing natural sources have emerged as viable and simple strategies for green NPs synthesis.[7−11] Intracellular growth of metallic NPs may be a unique and useful approach to overcome the space constraint of the NPs which are essential to an effective SERS dectection. Biosynthesis of NPs with different sizes, shapes, and compositions has been found in various microorganisms,[12−14] plants,[15] and mammalian cells.[16−18] In this case, the gold or silver ions diffused inside the cells are reduced into elemental metals by an intracellular redox system,[19] although the exact mechanism is still unknown. In human cells, the intracellularly grown gold NPs (IGAuNs) have been successfully served as nanosensors for SERS detection to elucidate the subcellular components localized in the cytoplasm and nucleus.[17]

Graphene, a novel two-dimensional carbon nanomaterial with excellent physical and chemical properties, has received remarkable attention since its discovery by Novoselov and Geim.[20] In biomedical applications, graphene and graphene oxide (GO) have been developed as promising nanobiomaterials for drug delivery, photothermal therapy, biocompatible scaffold, and biosensor.[21−24] Due to the ultrahigh surface area, GO is successfully used as a nanocarrier for delivery of aromatic drug molecules and nucleic acid via noncovalent $\pi-\pi$ stacking or hydrophobic interaction.[25−27] In our latest work, we demonstrated the ability of PEGylated nanographene oxide as a platform for combined drug delivery and photothermal tumor therapy.[28] Recently, GO/noble metal NPs composites have attracted overwhelming attention for their excellent catalytic, electronic, and optical properties.[29]

Received: August 18, 2012
Accepted: October 23, 2012
Published: October 23, 2012

Compared with Au or Ag NPs, the hybrids exhibit higher SERS activity, benefiting from the high affinity of GO to aromatic molecules.[30−33] To investigate the potential of GO/metal NPs in biomedicine, Ren et al. reported a self-assemble GO/PDDA/AgNPs for ultrasensitive SERS detection of folic acid in water or serum with a minimum-detected concentration up to 9 nM.[31] Nevertheless, the nanocomposites systhesized by chemical methods seem powerless in characterization of complex biological samples, as the related literature has not yet been reported.

Herein, a green and facile strategy was proposed for fast intracellular fabrication of GO/PVP/IGAuNs nanocomposites, in which poly(vinylpyrrolidone) (PVP)-functionalized GO served as an activator for IGAuNs biosynthesis. PVP, a nonionic, water-soluble, and nontoxic polymer surfactant, was often employed as stabilizing agent and coordinating agent for the synthesis of metal nanostructures with controlled size and shape.[34−36] On the other hand, PVP also served as a biocompatible stabilizer of GO in a physiological environment. Trace amounts of PVP delivered into the cell were enriched onto the huge surface of GO, which provided an atomic template to coordinate the reduction of gold ions into gold metals initiated by the intracellular redox system. The obtained GO/PVP/IGAuNs hybrids exhibited strong SERS activity to mammalian cells, indicating a great potential for biomedical applications.

EXPERIMENTAL SECTION

Materials. Chloroauric acid ($HAuCl_4{\cdot}4H_2O$) and poly(vinylpyrrolidone) (PVP, K10) were purchased from China National Medicine Corporation (Shanghai, China). Native graphite flake was purchased from Alfa Aesar. Dulbecco's modified Eagle's medium (DMEM) and fetal bovine serum (FBS) were obtained from GIBCO (Grand Island, NY, United States). Other reagents were of analytical grade and were used as received without further purification. Deionized water (Milli-Q System, Millipore, USA) was used in all experiments.

GO was synthesized from graphite flakes according to our previous work.[28] The as-prepared GO was then dissolved in water, yielding a stable yellow-brown dispersion. The obtained GO was then cracked by an ultrasonic probe at 700 W for 3 h. PVP-coated GO was obtained as follows: typically, 20 mg of PVP was added into 10 mL GO water solution (0.5 mg/mL) followed by a 30 min ultrasonic bath. The obtained GO-PVP mixture was then stirred at 50 °C for 18 h. The excess PVP was separated out by dialysis against deionized water. RGO-PVP was acquired via exposure of GO-PVP to hydrazine hydrate (80 wt %, 90 °C) for 1 h. One mM $HAuCl_4$ was prepared in phosphate-buffered saline (PBS, pH 7.4). Solutions of $HAuCl_4$ in PBS were stable for several months, which ruled out the possibility of autoreduction (Figure S1 of the Supporting Information). The as-prepared (R)GO-PVP solution and $HAuCl_4$ solution were filter-sterilized using MILLEX GV Durapore PVDF membrane filter (0.22 μm pore size) for use later.

Intracellular Growth of Gold Nanostructures. Human lung epithelial (A549), mouse mammary tumor (4T1), and human cervical cancer (HeLa) cells were cultured in DMEM supplemented with 10% FBS, penicillin (100 units/mL), and streptomycin (100 μg/mL) in 5% CO_2 and 95% air at 37 °C in a humidified incubator. The cells were seeded in cell-culture dishes (35 mm) with 2 mL of medium for 24 h to reach 85−90% confluence. The growth medium was then removed and the cells were washed with PBS three times. For biosynthesis of GO/PVP/IGAuNs, 2 mL of 1 mM $HAuCl_4$ and 40 μL of GO-PVP were added into the Petri dishes. Then, the cells were kept in an incubator (37 °C, 5% CO_2) for the growth of gold nanostructures. For the growth of IGAuNs, cells were exposed to 1 mM $HAuCl_4$.

Characterization of Gold Nanoparticles. The in situ TEM observation of gold nanostructures inside A549 cells was performed by a JEM-2100HR transmission electron microscopy (JEOL, Japan) operated at 100 kV equipped with an energy-dispersive X-ray (EDX) spectrum. The cells were harvested by a cell scraper and resuspended in PBS. Then the cells were washed three times by centrifugation (2000 rpm, 5 min). Precipitates were fixed in 3% glutaraldehyde in HEPES buffer (pH 7.4) for 2 h. After dehydration, the cells were embedded in Epoxy 618. Ultrathin sections of the A549 cells were acquired using an EM-UC6 microtome (Leica Co., Austria). Cells were stained by uranyl acetate and lead citrate prior to examination with TEM.

The UV−vis spectra of the A549 cells (resuspension in PBS) were measured by a UV−Vis spectrometer (NanoDrop, ND-1000). The X-ray powder diffraction (XRD) patterns of the A549 cells were recorded on a MSAL-XD2 X-ray diffractometer with Cu Kα radiation (36 kV, 20 mA, λ = 1.54051 Å).

SERS Measurements. For Raman detection, the cells precultured on quartz substrates were rinsed with PBS five times. The Raman spectroscopic measurements on ∼5 individual cells per group were conducted directly in the PBS buffer using a Renishaw inVia confocal Raman system (controlled by WiRE 3.2 software) coupled to a Leica DM 2500 microscope (Renishaw, Glouchestershire, United Kingdom). The spectrometer was equipped with a 785 nm near-IR semiconductor laser (∼250 mW). A 50× objective (NA 0.75) was used to focus the laser beam and to collect the Raman signal. The laser power on the sample was about 1.25 mW to avoid laser-induced heating. The size of the laser spot was about 1 μm. The Raman spectra were recorded in static mode for a 50 s laser exposure over a wavenumber range of 600−1700 cm^{-1}. All experiments were independently carried out at least five times. A well-established automated algorithm for autofluorescence background subtraction was applied to extract pure Raman spectra from the raw data.[37] Raman spectral maps were collected in the Streamline mode at a 30 s exposure time with a wavenumber center at 1200 cm^{-1} using a 100× objective (NA 0.85). SERS images of A549 cells were plotted by integrating the signal-to-baseline intensity in the spectral range between 600 and 1700 cm^{-1}.

RESULTS AND DISCUSSION

A549 cells were used as model cells. Figure 1 describes the optical micrographs of A549 cells treated with 1 mM $HAuCl_4$ in PBS (pH 7.4) with or without 10 μg/mL GO-PVP 24 h later. It can be seen that the cell contour is clearly visible, indicating the intracellular synthesis of nanoparticles.[16] The cells are stained result from the formation of gold nanoparticles. Some of the nanoparticles form aggregates with micrometer size, which are observable under the optical microscope (dark particles in Figure 1). Some gold nanostructures appear extracellularly which indicates that the reduction also exists in the extracellular matrix. The large number of dark particles in Figure 1b reveal the fast synthesis of gold nanostructures assisted by GO-PVP.

TEM analysis was performed to investigate the morphology of nanostructures and its distribution inside the cell. TEM

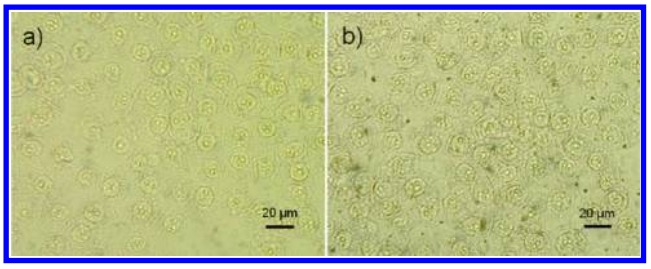

Figure 1. Optical micrographs of A549 cells incubated with PBS containing (a) 1 mM $HAuCl_4$ or (b) 1 mM $HAuCl_4$ and 10 μg/mL GO-PVP 24 h later.

images of ultrathin cross sections of A549 cells after 24 h of incubation with precursors clearly showed that the gold nanostructures are mainly located in the cytoplasm, although they are scattered throughout the cell (Figure 2). The data are consistent with the previous reports about IGAuNs.[16,17] The random distribution, which is significantly different from AuNPs taken up by way of endocytosis, makes the intracellularly grown gold naostructures more superior for SERS analysis. Some of the particles accumulate inside the cytoplasm due to the presence of various salts (Figure 2b). However, the number and morphologies of nanostructures vary significantly after the addition of trace amounts of GO-PVP (Figure 2, panels c and d). The growth of gold nanostructures is remarkably accelerated (Figure 2c), which can also be confirmed by the UV−vis spectra (Figure 3). The absorption

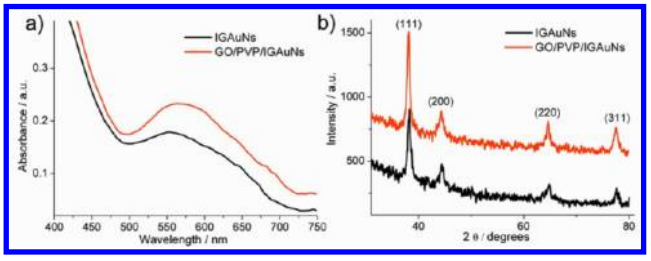

Figure 3. (a) UV−vis spectra and (b) XRD patterns of A549 cells contained with IGAuNs or GO/PVP/IGAuNs.

of GO/PVP/IGAuNs nanocomposites shows a little redshift, compared to that of IGAuNs (~550 nm). The XRD patterns for A549 cell samples (Figure 3b) show four remarkable peaks corresponding to (111), (200), (220), and (311), which are characteristic of gold lattice. The EDX spectrum of GO/PVP/

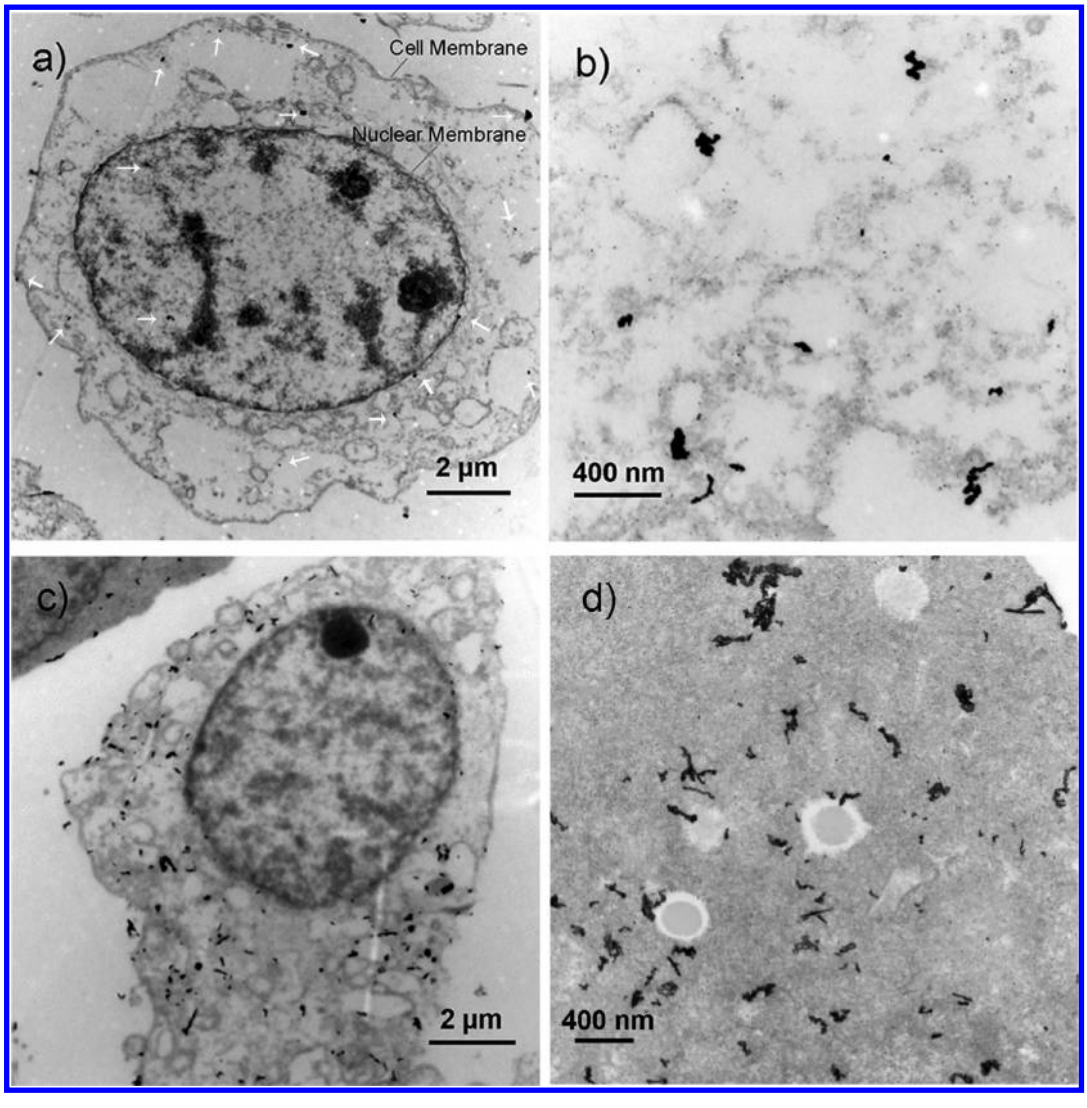

Figure 2. TEM images of A549 cells containing (a and b) IGAuNs and (c and d) GO/PVP/IGAuNs nanocomposites.

dx.doi.org/10.1021/ac3023907 | *Anal. Chem.* 2012, 84, 10338−10344

IGAuN nanocomposites also shows the presence of strong signals from the gold atoms (Figure 4).

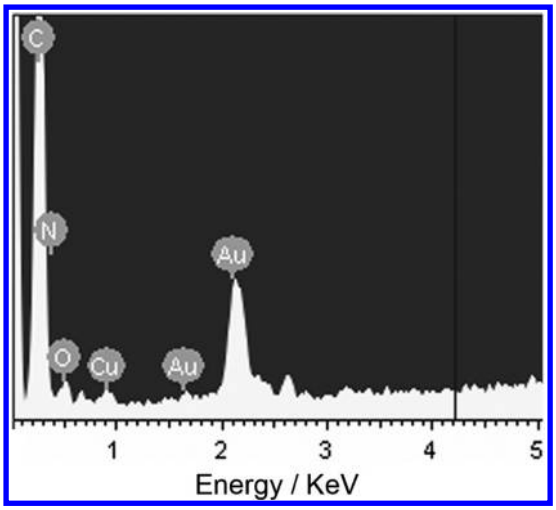

Figure 4. EDX spectrum of GO/PVP/IGAuNs in an A549 cell.

Figure 2, panels b and d show the high-magnification TEM images of the gold nanostructures. The shapes of the IGAuNs are irregular, and the sizes are less than 100 nm (Figure 2b), which are similar to the data reported by Anshup et al.[16], while GO/PVP/IGAuNs at a few hundred nanometers in size can be well-identified in Figure 2d. Interestingly, some of the composites show ribbonlike structures. The nanoribbons are prone to curl up inside the cell. However, we can not observe the filmlike structure of GO-PVP (Figure S2 of the Supporting Information), probably due to the low-electron density of GO. It is therefore difficult to distinguish GO from the cellular components in the TEM images.[38]

The Raman spectra of cells were collected using a commercial confocal Raman microspectrometer. As shown in Figure 5, no Raman signals are detected from the controls under our experimental condition (1% laser intensity, 50 s integration time). However, strong Raman signals of A549 cells can be observed in IGAuNs or GO/PVP/IGAuNs-induced SERS spectra. The SERS spectra (Figure 5a) clearly identify the important components such as proteins, nucleic acids, lipids, and carbohydrates. A comparison between the two SERS spectra, the Raman enhancement induced by GO/PVP/IGAuNs is about 5 times larger than that generated from IGAuNs. Moreover, a large amount of new Raman bands emerge in the hybrids-induced SERS spectrum. For example, 642 cm^{-1} (tyrosine C−C twisting), 692 cm^{-1} (cytosine), 855 cm^{-1} (tyrosine ring breathing, proline C−C stretching), 934 cm^{-1} (α helix C−C backbone stretching, glycosidic bond C−O−C vibration), 1063 cm^{-1} (protein C−N stretching, lipid chain C−C stretching), and 1498 cm^{-1} (guanine and adenine).[39−42] The SERS effect of GO/PVP/IGAuNs is common to several mammalian cells. Intense Raman signals are also observed in the SERS spectra of 4T1 or HeLa cells (Figure S3 of the Supporting Information), indicating the widespread biomedical applications of GO/PVP/IGAuNs as SERS-active probes.

Some of the nanoparticles form aggregates which have been proposed as superior SERS substrates.[43] SERS spectra were also collected from the dark spots (Figure 1b) believed to be GO/PVP/IGAuNs aggregates. It can be seen that the average SERS signal strength induced by the aggregates is much larger (~2 times enhancement) than that measured from the regions with no aggregates (Figure S4 of the Supporting Information). In addition, more Raman information can be observed in the SERS spectrum generated from the aggregates.

We further investigated the time-dependent SERS effects of the gold nanostructures grown intracellularly. Raman spectra of A549 cells were collected after incubation with the precursors for 12, 15, and 18 h. No Raman signals are detected at 12 h (Figure S5 of the Supporting Information). However, a remarkable difference appears at 15 h. As shown in Figure 5b, no distinguishable Raman peak is acquired from the A549 cells after 15 h of treatment with 1 mM $HAuCl_4$, while the Raman fingerprints of A549 cells are well reproduced in the GO/PVP/IGAuN-induced SERS spectrum. This result suggests that the strategy of fast biosynthesis of gold nanostructures assisted by GO-PVP facilitates the application of the SERS technique for early diagnosis of cancer.

The intracellularly grown gold nanostructures are indeed suitable for SERS detection of cellular components due to their extensive distribution inside the cell. SERS spectra were measured from A549 cells at positions corresponding to the cytoplasm, nucleoplasm, and nucleolus. As shown in Figure 6, a fingerprint-like SERS spectrum is observed in every region,

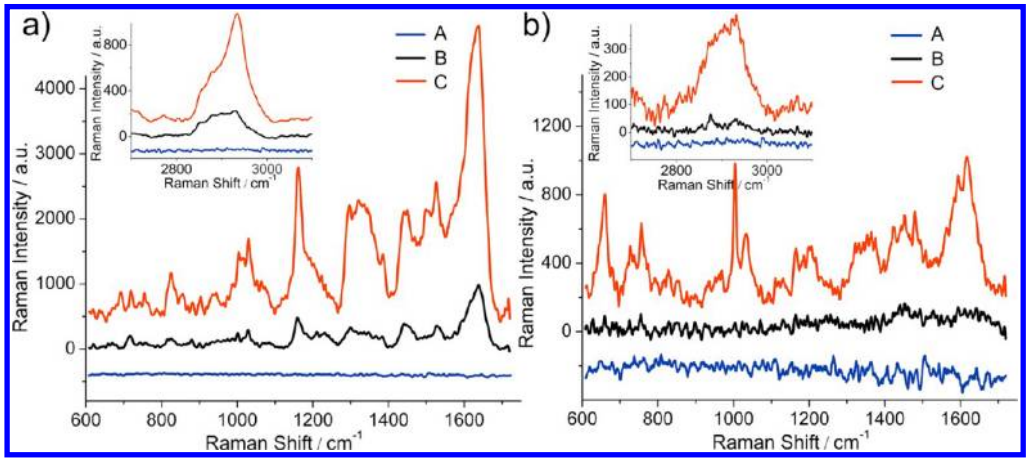

Figure 5. (A) Normal Raman and (B, IGAuNs and C, GO/PVP/IGAuNs) SERS spectra of A549 cells after (a) 24 h or (b) 15 h incubation with precursors.

dx.doi.org/10.1021/ac3023907 | Anal. Chem. 2012, 84, 10338−10344

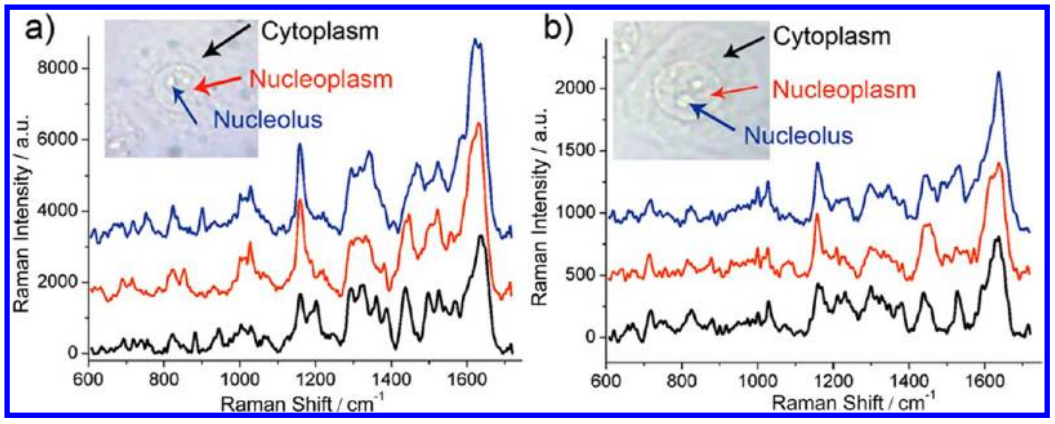

Figure 6. (a, GO/PVP/IGAuNs and b, IGAuNs) SERS spectra of A549 cells collected from the regions corresponding to the cytoplasm, nucleoplasm, and nucleolus.

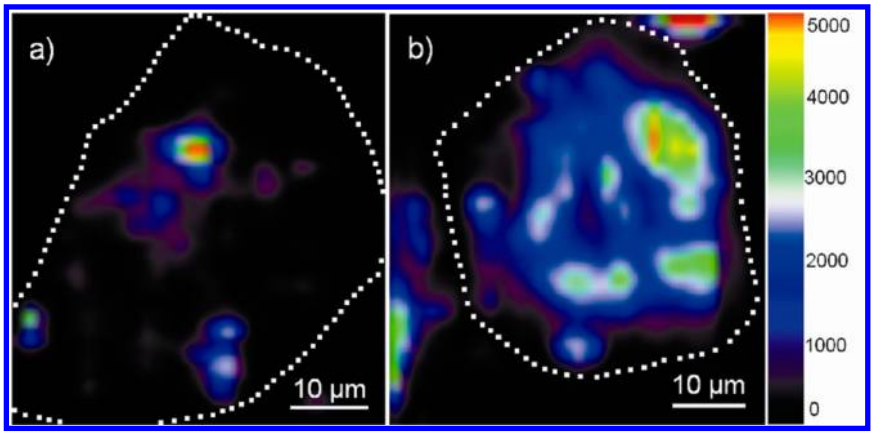

Figure 7. Typical SERS images of A549 cells contained with (a) IGAuNs or (b) GO/PVP/IGAuNs, showing the distribution of gold nanostructures inside the cell. The dotted lines in the images are drawn to indicate the boundaries of select cells.

which is consistent with the previous report.[17] Compared to the SERS spectra collected from the cells treated with IGAuNs (Figure 6b), the GO/PVP/IGAuN-induced SERS spectra exhibit similar Raman spectral features but distinctly stronger signals (Figure 6a). Comparisons among the three spectral lines collected from the cells treated with GO/PVP/IGAuNs show that the SERS spectral pattern acquired from the cytoplasm is, to a certain degree, different from the spectra collected from the nucleoplasm and nucleolus, in accordance with the diverse biochemical composition between the cytoplasm and the nucleus (Figure 6a). Raman bands associated with nucleic acids at 786 cm^{-1} (uracil, thymine, and cytosine; O−P−O stretching), 902 cm^{-1} (ribose-phosphate), 1018 cm^{-1} (C−O stretching), and 1344 cm^{-1} (guanine and adenine) are more intense in the spectra collected from the nucleus. In comparison with the spectrum of nucleolus, more Raman signatures corresponding to proteins (tyrosine and proline at 855 cm^{-1}, CH_3 deformation at 1384 cm^{-1}, CH_2 deformation at 1440 cm^{-1}, and amide II at 1560 cm^{-1}) are observed in the nucleoplasm, implying the nucleoskeleton. The SERS spectrum acquired from the cytoplasm displays the most abundant chemical information. The Raman bands assigned to proteins, lipids, and carbohydrates at 882 cm^{-1} (disaccharide, C−O−C skeletal mode), 944 cm^{-1} (α-helix, C−C stretching), 1201 cm^{-1} (tyrosine and phenylalanine), 1360 cm^{-1} (CH_2/CH_3 twisting and wagging in protein), and 1440 cm^{-1} (CH_2 deformation in protein and lipid) are exclusive in the spectrum measured from the cytoplasm.

SERS mapping with a lateral resolution of 0.7 μm was performed across the A549 cells to further illustrate the location of gold nanostructures inside the cell. Figure 7 shows the false-color SERS images of A549 cells plotted by integrating the signals from 600 to 1700 cm^{-1}, which represents the distribution of gold nanostructures within a cross-section of the cell. The strongest Raman signals in the figures are considered as the gold aggregates. A nonuniform distribution of IGAuNs is displayed in Figure 7a, which may be largely attributed to the low yield of the elemental metal. However, the SERS signals induced by GO/PVP/IGAuNs with high intensities are observed almost throughout the cell (Figure 7b), indicating a uniform intracellular distribution of the hybrids. The data, in accordance with the TEM images (Figure 2), confirm that the intracellular growth of gold nanostructures can be accelerated by GO-PVP, which is particularly helpful for the SERS detection of cellular components.

The polymer (PVP) coordinates the synthesis of the nanocomposites. To gain insight into the exact role of GO in the formation of GO/PVP/IGAuNs, A549 cells were also treated with PVP and $HAuCl_4$ without the presence of GO. Comparisons were made among the SERS spectra of A549 cells induced by IGAuNs, PVP/IGAuNs, and GO/PVP/IGAuNs (Figure S6 of the Supporting Information). In the cytoplasm, the PVP/IGAuN-induced SERS spectrum exhibits much stronger and more plentiful signals than that generated from IGAuNs, although the signals are still weaker than that induced by GO/PVP/IGAuNs. However, the SERS enhancement of

PVP/IGAuNs becomes less effective in the nucleus, mainly ascribed to the low delivery efficiency of PVP into the nucleus. In contrast, extremely high SERS enhancement of GO/PVP/IGAuNs is still observed in the nucleoplasm or nucleolus. We consider that GO here serves as a nanocarrier for the enrichment of PVP, which largely promotes the formation of gold nanostructures. The role is particularly important in the nucleus, a natural barrier for allogenic materials. GO enriched with PVP in the nucleus provides a nanofactory for the formation of GO/PVP/IGAuNs, thus inducing the strong SERS signals.

Furthermore, PVP-functionalized reduced graphene oxide (RGO), prepared via exposure of GO-PVP to hydrazine hydrate, was acquired to investigate the influence of chemical reduction of GO on the SERS effect. As shown in Figure S7 of the Supporting Information, the SERS spectrum of A549 cells induced by RGO/PVP/IGAuNs is severely interfered by the D band and G band of RGO. It is believed that RGO/PVP/IGAuNs significantly enhance the Raman signals of RGO which drown out the signals of the cellular components.

CONCLUSION

In conclusion, we have presented a novel and green strategy for the fast intracellular synthesis of gold nanostructures directed by PVP-functionalized GO. Optical microscopy imaging and TEM analysis demonstrated that the growth of GO/PVP/IGAuNs was faster than IGAuNs. The hybrids randomly scattered throughout the cell. The obtained nanocomposites could serve as excellent SERS probes for ultrasensitive detection of cellular components of mammalian cells (A549, 4T1, and HeLa cells). The SERS signals could be acquired as early as 15 h, indicating the potential for early diagnosis of cancer. Owing to the extensive intracellular distribution, biochemical composition in the regions corresponding to the cytoplasm, nucleoplasm, and nucleolus could be well-distinguished in the SERS spectra induced by the nanocomposites. SERS mapping of A549 cells showed a uniform distribution of SERS signals, further revealing the good SERS activity of GO/PVP/IGAuNs. Furthermore, the SERS activity of GO/PVP/IGAuNs was strongly dependent on the degree of chemical reduction of GO, which could weaken the SERS effect of the hybrids. Generally speaking, this facile and green strategy for rapid intracellular growth of GO/PVP/IGAuNs provides great potential for SERS detection and other metal-based biomedical applications.

ASSOCIATED CONTENT

Supporting Information

Additional information as noted in text. This material is available free of charge via the Internet at http://pubs.acs.org.

AUTHOR INFORMATION

Corresponding Author

*E-mail: ann@scnu.edu.cn.

Notes

The authors declare no competing financial interest.

ACKNOWLEDGMENTS

This work was supported by the National Natural Science Foundation of China (61275187), Specialized Research Fund for the Doctoral Program of Higher Education of China (20114407110001), the Natural Science Foundation of Guangdong Province (9251063101000009), and the cooperation project in industry, education, and research of Guangdong province and Ministry of Education of China (2011A090200011).

REFERENCES

(1) Jarvis, R. M.; Law, N.; Shadi, I. T.; O'Brien, P.; Lloyd, J. R.; Goodacre, R. *Anal. Chem.* **2008**, *80*, 6741−6746.
(2) Auchinvole, C. A.; Richardson, P.; McGuinnes, C.; Mallikarjun, V.; Donaldson, K.; McNab, H.; Campbell, C. J. *ACS Nano* **2012**, *6*, 888−896.
(3) Ando, J.; Fujita, K.; Smith, N. I.; Kawata, S. *Nano Lett.* **2011**, *11*, 5344−5348.
(4) Samanta, A.; Maiti, K. K.; Soh, K.-S.; Liao, X.; Vendrell, M.; Dinish, U. S.; Yun, S.-W.; Bhuvaneswari, R.; Kim, H.; Rautela, S.; Chung, J.; Olivo, M.; Chang, Y.-T. *Angew. Chem., Int. Ed.* **2011**, *50*, 6089−6092.
(5) Campion, A.; Kambhampati, P. *Chem. Soc. Rev.* **1998**, *27*, 241−250.
(6) Chithrani, B. D.; Ghazani, A. A.; Chan, W. C. *Nano Lett.* **2006**, *6*, 662−668.
(7) Das, S. K.; Dickinson, C.; Lafir, F.; Brougham, D. F.; Marsili, E. *Green Chem.* **2012**, *14*, 1322−1334.
(8) Mandal, D.; Bolander, M. E.; Mukhopadhyay, D.; Sarkar, G.; Mukherjee, P. *Appl. Microbiol. Biotechnol.* **2006**, *69*, 485−492.
(9) Iravani, S. *Green Chem.* **2011**, *13*, 2638−2650.
(10) Sicard, C.; Brayner, R.; Margueritat, J.; Hemadi, M.; Coute, A.; Yepremian, C.; Djediat, C.; Aubard, J.; Fievet, F.; Livage, J.; Coradin, T. *J. Mater. Chem.* **2010**, *20*, 9342−9347.
(11) Li, S.; Shen, Y.; Xie, A.; Yu, X.; Qiu, L.; Zhang, L.; Zhang, Q. *Green Chem.* **2007**, *9*, 852−858.
(12) Klaus, T.; Joerger, R.; Olsson, E.; Granqvist, C. G. *Proc. Natl. Acad. Sci. U.S.A.* **1999**, *96*, 13611−13614.
(13) Mukherjee, P.; Ahmad, A.; Mandal, D.; Senapati, S.; Sainkar, S. R.; Khan, M. I.; Parishcha, R.; Ajaykumar, P. V.; Alam, M.; Kumar, R.; Sastry, M. *Nano Lett.* **2001**, *1*, 515−519.
(14) Ravindranath, S. P.; Henne, K. L.; Thompson, D. K.; Irudayaraj, J. *ACS Nano* **2011**, *5*, 4729−4736.
(15) Gardea-Torresdey, J. L.; Gomez, E.; Peralta-Videa, J. R.; Parsons, J. G.; Troiani, H.; Jose-Yacaman, M. *Langmuir* **2003**, *19*, 1357−1361.
(16) Anshup, A.; Venkataraman, J. S.; Subramaniam, C.; Kumar, R. R.; Priya, S.; Kumar, T. R.; Omkumar, R. V.; John, A.; Pradeep, T. *Langmuir* **2005**, *21*, 11562−11567.
(17) Shamsaie, A.; Jonczyk, M.; Sturgis, J.; Paul Robinson, J.; Irudayaraj, J. *J. Biomed. Opt.* **2007**, *12*, 020502.
(18) Larios-Rodriguez, E.; Rangel-Ayon, C.; Castillo, S. J.; Zavala, G.; Herrera-Urbina, R. *Nanotechnology* **2011**, *22*, 355601.
(19) Duran, N.; Marcato, P. D.; Alves, O. L.; Souza, G. I.; Esposito, E. *J. Nanobiotechnol.* **2005**, *3*, 8.
(20) Novoselov, K. S.; Geim, A. K.; Morozov, S. V.; Jiang, D.; Zhang, Y.; Dubonos, S. V.; Grigorieva, I. V.; Firsov, A. A. *Science* **2004**, *306*, 666−669.
(21) Li, J. L.; Bao, H. C.; Hou, X. L.; Sun, L.; Wang, X. G.; Gu, M. *Angew. Chem., Int. Ed.* **2012**, *51*, 1830−1834.
(22) Zhang, L.; Xia, J.; Zhao, Q.; Liu, L.; Zhang, Z. *Small* **2010**, *6*, 537−544.
(23) Nayak, T. R.; Andersen, H.; Makam, V. S.; Khaw, C.; Bae, S.; Xu, X.; Ee, P. L.; Ahn, J. H.; Hong, B. H.; Pastorin, G.; Ozyilmaz, B. *ACS Nano* **2011**, *5*, 4670−4678.
(24) Wang, H.; Zhang, Q.; Chu, X.; Chen, T.; Ge, J.; Yu, R. *Angew. Chem., Int. Ed.* **2011**, *50*, 7065−7069.
(25) Liu, Z.; Robinson, J. T.; Sun, X.; Dai, H. *J. Am. Chem. Soc.* **2008**, *130*, 10876−10877.
(26) Misra, S. K.; Kondaiah, P.; Bhattacharya, S.; Rao, C. N. R. *Small* **2012**, *8*, 131−143.
(27) Zhang, L.; Lu, Z.; Zhao, Q.; Huang, J.; Shen, H.; Zhang, Z. *Small* **2011**, *7*, 460−464.

(28) Zhang, W.; Guo, Z.; Huang, D.; Liu, Z.; Guo, X.; Zhong, H. *Biomaterials* **2011**, *32*, 8555−8561.
(29) Huang, X.; Qi, X.; Boey, F.; Zhang, H. *Chem. Soc. Rev.* **2012**, *41*, 666−686.
(30) Zhang, Z.; Xu, F.; Yang, W.; Guo, M.; Wang, X.; Zhang, B.; Tang, J. *Chem. Commun.* **2011**, *47*, 6440−6442.
(31) Ren, W.; Fang, Y.; Wang, E. *ACS Nano* **2011**, *5*, 6425−6433.
(32) Liu, X.; Cao, L.; Song, W.; Ai, K.; Lu, L. *ACS Appl. Mater. Interfaces* **2011**, *3*, 2944−2952.
(33) Huang, J.; Zhang, L.; Chen, B.; Ji, N.; Chen, F.; Zhang, Y.; Zhang, Z. *Nanoscale* **2010**, *2*, 2733−2738.
(34) Sun, Y. G.; Xia, Y. N. *Science* **2002**, *298*, 2176−2179.
(35) Jeon, S.-H.; Xu, P.; Zhang, B.; Mack, N. H.; Tsai, H.; Chiang, L. Y.; Wang, H.-L. *J. Mater. Chem.* **2011**, *21*, 2550−2554.
(36) Quaresma, P.; Soares, L.; Contar, L.; Miranda, A.; Osorio, I.; Carvalho, P. A.; Franco, R.; Pereira, E. *Green Chem.* **2009**, *11*, 1889−1893.
(37) Zhao, J.; Lui, H.; McLean, D. I.; Zeng, H. *Appl. Spectrosc.* **2007**, *61*, 1225−1232.
(38) Mu, Q.; Su, G.; Li, L.; Gilbertson, B. O.; Yu, L. H.; Zhang, Q.; Sun, Y.-P.; Yan, B. *ACS Appl. Mater. Interfaces* **2012**, *4*, 2259−2266.
(39) Notingher, I.; Verrier, S.; Haque, S.; Polak, J. M.; Hench, L. L. *Biopolymers* **2003**, *72*, 230−240.
(40) Xie, W.; Wang, L.; Zhang, Y.; Su, L.; Shen, A.; Tan, J.; Hu, J. *Bioconjugate Chem.* **2009**, *20*, 768−773.
(41) Jess, P. R. T.; Smith, D. D. W.; Mazilu, M.; Dholakia, K.; Riches, A. C.; Herrington, C. S. *Int. J. Cancer* **2007**, *121*, 2723−2728.
(42) Otto, C.; van den Tweel, T. J. J.; de Mul, F. F. M.; Greve, J. *J. Raman Spectrosc.* **1986**, *17*, 289−298.
(43) Kneipp, J.; Kneipp, H.; McLaughlin, M.; Brown, D.; Kneipp, K. *Nano Lett.* **2006**, *6*, 2225−2231.